Journal of Colloid and Interface Science 536 (2019) 499–506

Contents lists available at ScienceDirect

Journal of Colloid and Interface Science

journal homepage: www.elsevier.com/locate/jcis

Regular Article

Capillary rise of polydimethylsiloxane around a poly(ethylene terephthalate) fiber versus viscosity: Existence of a sharp transition in the dynamic wetting behavior

Yichuan Zhang [a,b,*], Sébastien Moins [c], Olivier Coulembier [c], David Seveno [a], Joël De Coninck [b]

[a] Department of Materials Engineering, KU Leuven, 3001 Leuven, Belgium
[b] Laboratory of Surface and Interfacial Physics, Université de Mons, 7000 Mons, Belgium
[c] Laboratory of Polymeric and Composite Materials, Center of Innovation and Research in Materials and Polymers, Université de Mons, 7000 Mons, Belgium

GRAPHICAL ABSTRACT

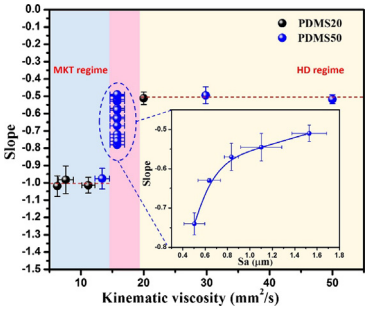

ARTICLE INFO

Article history:
Received 13 September 2018
Revised 25 October 2018
Accepted 25 October 2018
Available online 26 October 2018

Keywords:
Capillary rise
Dynamic contact angle
Molecular-kinetic theory
Hydrodynamic approach

ABSTRACT

Hypothesis: Since the emergence of the molecular-kinetic theory and the hydrodynamic approach, it is generally accepted that the displacement of the contact line is controlled by the viscous or frictional channel of energy dissipation for respectively high-viscosity and low-viscosity liquids. However, how the dissipation switches from one channel to another is still unknown. We therefore hypothesized that, by progressively changing the viscosity of a liquid, a better understanding of the underlying mechanism driving this wetting dynamic transition would be obtained.
Experiments: Performing capillary rise experiments of polydimethylsiloxane on a poly(ethylene terephthalate) fiber at different temperatures, i.e. at different liquid viscosities, we characterized the transition between the viscous and frictional regimes. The fiber surface topography was also characterized and its effect on the wetting dynamics was quantified.
Findings: The wetting dynamics switched from one regime to the other in a very short viscosity interval. Besides, the wetting behavior in the transition region is sensitive to the fiber surface topography. The presence or the absence of a liquid rim ahead of the contact line actually determines the dominant channel of dissipation.

1. Introduction

The considerable interests in wetting dynamics arise from their great importance in many processes, such as painting, adhesion, oil recovery and liquid-based microfluidic systems. Therefore, the

* Corresponding author at: Department of Materials Engineering, KU Leuven, 3001 Leuven, Belgium and Laboratory of Surface and Interfacial Physics, Université de Mons, 7000 Mons, Belgium.
E-mail address: yichuan.zhang@kuleuven.be (Y. Zhang).

https://doi.org/10.1016/j.jcis.2018.10.082
0021-9797/

wetting topic has been studied extensively, from both numerical and experimental aspects [1–3]. To describe the underlying mechanisms controlling the contact line dynamics, two main theoretical approaches, i.e., the hydrodynamic approach (HD) and the molecular-kinetic theory (MKT), have been proposed. The two models differ from each other both in terms of their conceptual frameworks and in the consideration of the channel of energy dissipation [2–6]. The HD emphasizes the viscous dissipation within the wedge of moving liquid close to the moving contact line [7–10], whereas the MKT proposed by Blake and Hayes concentrates on the effective channel of dissipation stemming from the frictional processes in the vicinity of the contact line [11–14]. When the two models are applied to predict the spreading of a drop on a flat surface with small advancing contact angle (θ_t), the hydrodynamic regime can be characterized asymptotically by $\theta_t \sim t^{-3/10}$ (so-called Tanner's law) [9,13,15] and the frictional regime leads to a different behavior, namely $\theta_t \sim t^{-3/7}$ [13,16,17]. It implies that the difference between the two regimes is not obvious on flat surfaces. This is a reason why both HD and MKT sometimes can be equally well fitted for a given set of experimental results simultaneously, making the identification of the dominant channel of dissipation ambiguous [18,19]. For the fiber geometry, θ_t varies as $\theta_t \sim t^{-1/2}$ and $\theta_t \sim t^{-1}$ for the HD [20,21] and MKT [22,23], respectively. It suggests that fiber geometry has the advantage to enhance the difference between the two models and helps to distinguish between the dissipation regimes.

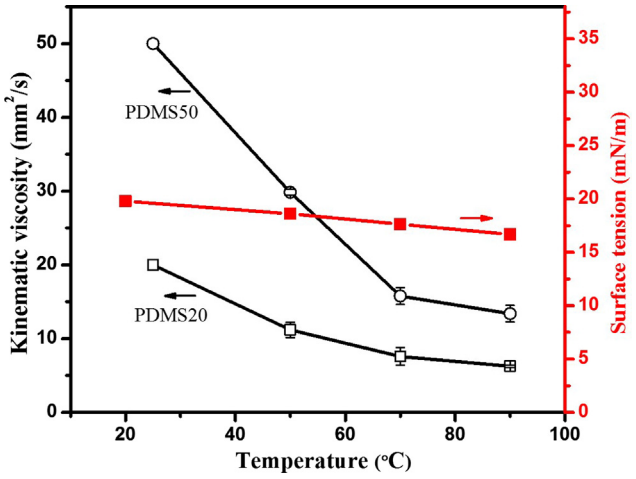

Fig. 1. Kinematic viscosity and surface tensions for PDMS20 and PDMS50 at different temperatures.

An emerging point of view that is gaining increasing ground is that both frictional and viscous dissipations play a role in the spreading process [1,13,24]. This statement triggers the elaboration of combined models, such as the models of Petrov and Petrov [25], Brochard-Wyart and de Gennes [26], de Ruijter and De Coninck, et al. [27]. However, at this stage, a unified approach describing the wetting dynamics of liquid is still missing. It is generally accepted that the viscous dissipation is the main channel of dissipation for high-viscosity systems and the frictional dissipation drives the low-viscosity liquid dynamics [23,28]. Intuitively, there should be a transition between the two models since the channel of dissipation is viscosity-dependent, which has been demonstrated experimentally in previous works [23,29]. This will raise a more fundamental question on how energy dissipation switches from one channel of dissipation to the other showing a smooth or sharp transition over short or long interval of viscosity. This unsolved challenge links the two main theoretical models with different theoretical bases in the field of dynamic wetting. Until this question is resolved experimentally or numerically, our understanding of the switch between different channels of dissipation is still rudimentary and developing a unified model remains elusive.

In the present work, we present experimental results of wetting dynamics of polydimethylsiloxane (PDMS) around a poly(ethylene terephthalate) (PET) fiber from an infinite reservoir at different temperatures. Two types of PDMS with kinematic viscosities of 20 mm^2/s (PDMS20) and 50 mm^2/s (PDMS50) at room temperature are selected based on the fact that both PDMS liquids follow the HD model [23] and their viscosities can be fine-tuned by varying temperature. The primary aim is to explore the transition between the two different dissipation mechanisms, and to provide an insight into the role of surface topography of fiber substrate in the wetting process.

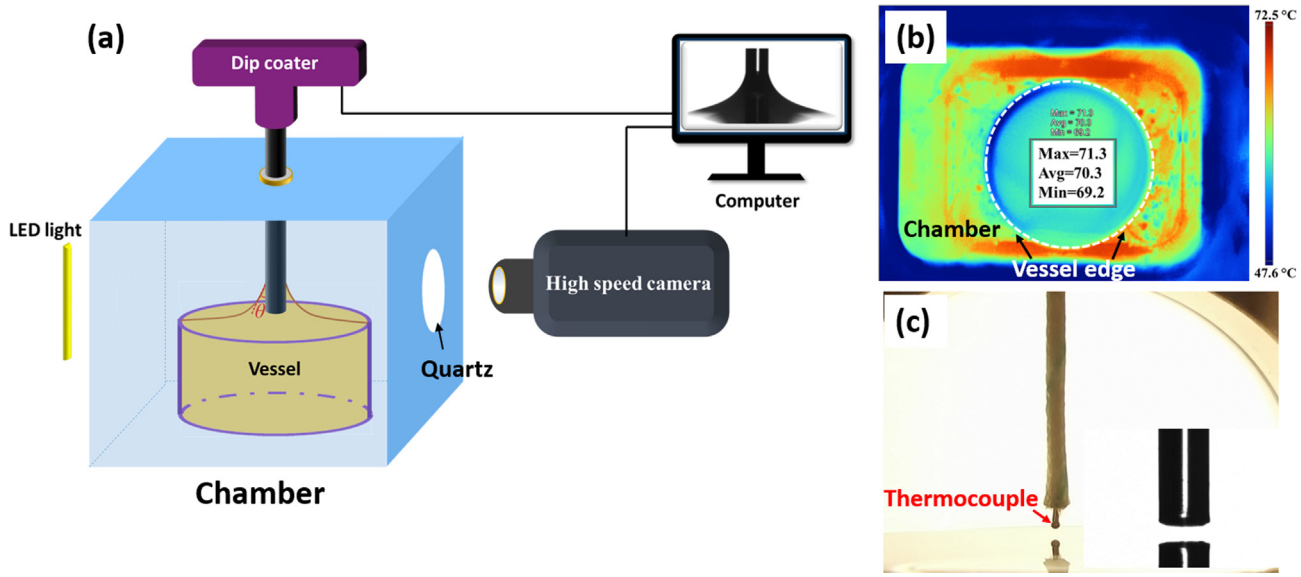

Fig. 2. (a) Schematic of the experimental setup. (b) Temperature mapping of an infrared image (top view) focusing on the PDMS liquid surface in the vessel within the chamber. (c) Optical image of an additional thermocouple above the liquid surface measuring the temperature of the fiber before contacting the liquid; The inset shows a fiber suspended for 40 min before contacting the liquid surface.

2. Materials and methods

2.1. Materials

The substrate is a PET fiber with 0.8 mm diameter from Goodfellow, which undergoes a rigorous cleaning procedure before use, as described previously [23,29]. The PDMS20 and PDMS50 liquids are linear polymer from Sigma-Aldrich Chemical co. PDMS20 and PDMS50 have a number-average molecular weight of 1678 and 3158 g/mol, respectively, measured by a gel permeation chromatography (GPC) method (Fig. S1 in the supplementary material).

2.2. Viscosity and surface tension measurement

A Brookfield DV-II+ PRO digital viscometer was used to measure viscosities of PDMS20 and PDMS50 liquids at different temperatures. The pendant drop method was used to measure the liquid/-vapor surface tensions by a Krüss drop-shape analyzer at 20 °C. At other temperatures, surface tensions were obtained by using a temperature coefficient $d\gamma/dT = -0.048$, with γ the liquid/vapor surface tension and T the temperature, a standard value for PDMS liquid [30]. Fig. 1 shows the values of the surface tension and kinematic viscosity (the ratio of the dynamic viscosity to the liquid

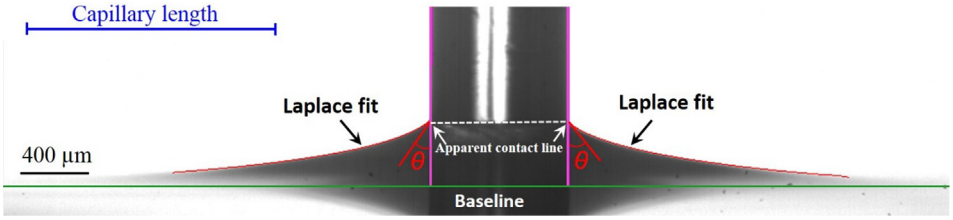

Fig. 3. A typical example of a contact angle measurement for PDMS50 at 90 °C. The best Laplace's fit of the liquid/air interface gives $\theta = 57.7 \pm 0.4°$.

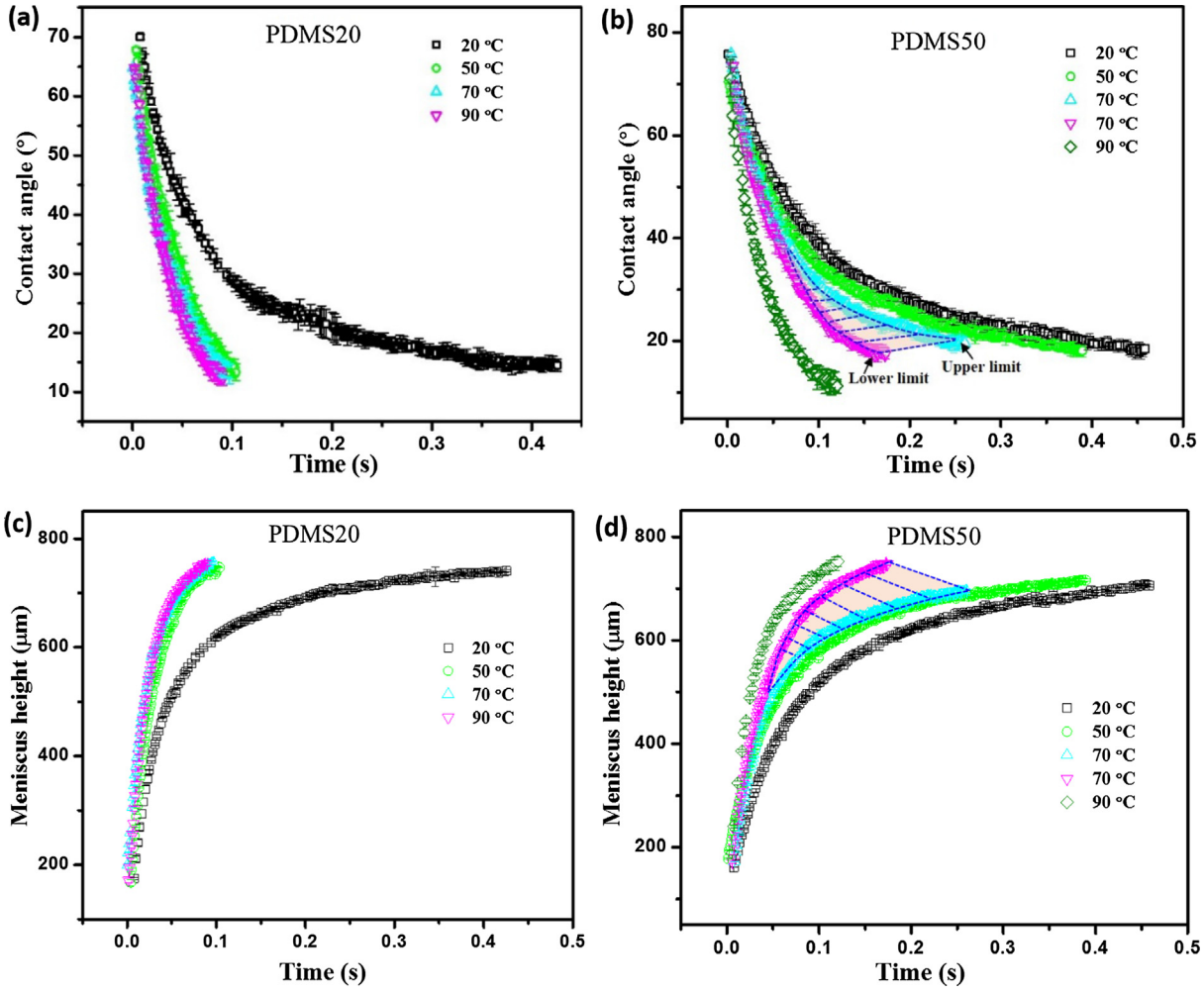

Fig. 4. Contact angle relaxation and meniscus height dynamics at different temperatures for PDMS20 (a and c) and PDMS50 (b and d). For PDMS50 at 70 °C, the upper and lower limiting dynamics enveloping all the others are shown (dotted blue lines). (For interpretation of the references to colour in this figure legend, the reader is referred to the web version of this article.)

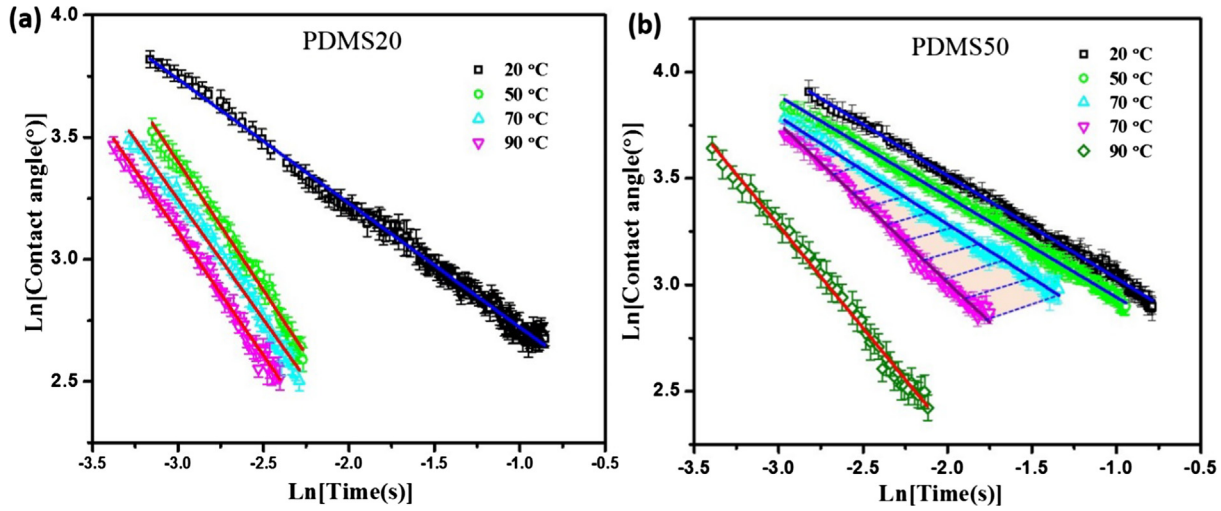

Fig. 5. Late stage contact angle dynamics versus time for PDMS20 (a) and PDMS50 (b) on a logarithmic scale. The solid lines correspond to the best linear fits.

density). It suggests that the viscosity values decrease dramatically with increasing temperature while surface tension values are nearly constant. Besides, the interfacial interaction between PET and PDMS nearly does not change with temperature (see Text S2 in the supplementary material).

2.3. Dynamic wetting measurements at different temperatures

The experimental system consists of a temperature-controlled chamber (Ramé-Hart instrument co.), a dip coater and a high speed camera (C-MOS camera, Vosskühler HCC-1000), as illustrated in Fig. 2a. The chamber shows excellent accuracy on temperature [18] which allows a precise control of the liquid surface temperature as shown in Fig. 2b (calibrated by a Fluke infrared camera). To consider the possible existence of temperature gradient along the meniscus profile, an additional thermocouple (Fig. 2c) is used to measure the temperature of the PET fiber. It shows a good agreement with the temperature of the liquid surface when the thermocouple is suspended above the liquid surface at a height of 0.8 mm for 40 min. This height is similar to the height of a static meniscus made by PDMS liquids around the fiber (see Fig. 4c and d). The process of capillary rise is then considered to be temperature-homogeneous. Besides, it is confirmed by FTIR-ATR (Fig. S2) that PDMS20 does not evaporate at 90 °C within 40 min.

The experimental procedure is as follows. The fiber attached to a dip coater is allowed to move down into the liquid reservoir with a controlled velocity. The downward motion (5 mm/min) of the sample is moved to the position of around 0.8 mm above the liquid surface at the target temperature and the sample is kept there for 40 min (illustrated in the inset of Fig. 2c). Then the fiber is moved downwards and it is stopped immediately when the fiber and liquid surface contact each other. The high speed camera records the dynamic process of capillary meniscus profile with a LED light (see Fig. 2a). The successive images are carefully checked when the meniscus rise starts. The capillary rise experiments were repeated more than 5 times for each PDMS at every temperature.

The capillary length, Bond number and capillary number of PDMS20 and PDMS50 are summarized in Table S3 in supplementary material. Clanet and Quéré [21] suggested that the fiber can be treated as a planar surface if *Bo* is larger than one unity. The value of *Bo* in Table S3 ranges 0.27 from 0.30, indicating that the filament should be considered as a cylinder. Besides, the PDMS liquid/vapor interface has a quasi-static profile and follows Laplace's equation since the values of capillary number do not exceed 0.03 at different temperatures. Fig. 3 presents an example of a contact angle measurement, in which a solution of Laplace's equation is adjusted to fit the shape of the liquid/vapor interface to obtain the contact angle and the meniscus height [31].

Table 1
Slopes of the different contact angle dynamics for PDMS20 and PDMS50 at different temperatures. The slopes cannot be simply averaged for PDMS50 at 70 °C due to their large scatter.

Samples	Temperature (°C)	Slope	Adj. R-Square
PDMS20	20	−0.51 ± 0.04	0.995
	50	−1.01 ± 0.05	0.996
	70	−0.98 ± 0.08	0.986
	90	−1.02 ± 0.06	0.992
PDMS50	20	−0.52 ± 0.03	0.996
	50	−0.50 ± 0.05	0.997
	70	/	/
	90	−0.98 ± 0.06	0.993

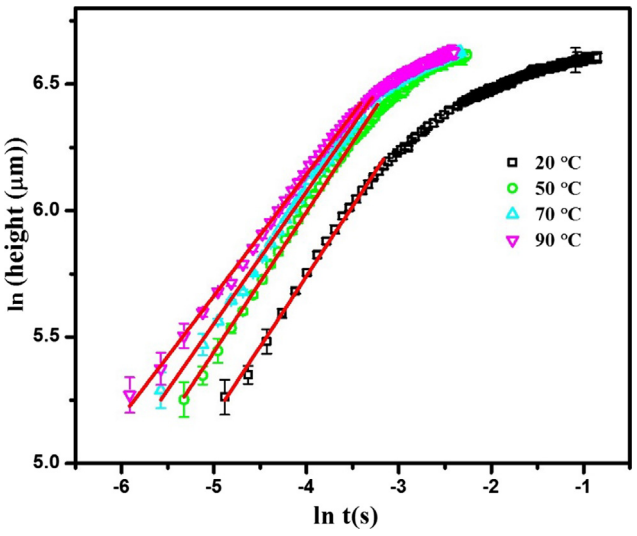

Fig. 6. Meniscus height dynamics vs time for PDMS20 at different temperatures on a logarithmic scale. The inertial contribution is modelled by Eq. (6). The solid lines correspond to the best linear fits with a slope of 0.554 (R^2 = 0.996), 0.552 (R^2 = 0.987), 0.522(R^2 = 0.997) and 0.479 (R^2 = 0.998) for 20, 50, 70 and 90 °C, respectively.

2.4. SEM analysis

The surface morphology of the PET fiber was observed in a Hirox SH-3000 scanning electron microscope (SEM) (Hirox company, Japan) with a voltage of 15 kV. Prior to SEM observation, the surfaces were sputtered with gold in Denton Desk V Sample Preparation system (Denton Vacuum L.L.C., USA)

2.5. 3D Optical profiler analysis

The 3D Optical Profiler (Sensofar-Tech, S.L., Spain) combing confocal and interferometry techniques was employed to characterize the roughness of the fiber surface. The values of roughness can be obtained by the analysis of the 3D Optical Profiler images using software SPIP 5.1.1. For every fiber, more than 3 different areas ($84.7 \times 84.7\ \mu m^2$) were characterized (these areas were wetted by the PDMS liquids during the capillary rise experiments).

2.6. Theoretical considerations

The de Ruijter combined model [27] simultaneously considering the viscous dissipation (HD) and the frictional dissipation (MKT) is employed to distinguish the dominant channels of dissipation. Since the substrate is a fiber and the initial de Ruijter combined model [27] is for a flat substrate, the de Ruijter combined model for fiber geometry extended by Seveno et al. [22,23] is considered here. It predicts dynamic contact angle θ_t varies as a function of the contact line velocity V

$$V = \frac{dy_t}{dt} = \frac{\gamma(\cos\theta_0 - \cos\theta_t)}{\zeta + \frac{6\eta}{\theta_t}\ln\left(\frac{x_{max}}{x_{min}}\right)} \tag{1}$$

where y_t is meniscus height, γ is the surface tension of liquid, θ_0 is the equilibrium contact angle on the fiber, η is the dynamic viscosity, ζ is the contact line friction per unit length of the contact line, x_{max} is in the range of the capillary length and x_{min} is of molecular size. This logarithm factor is generally approximated to 12 [32]. Assuming that values of θ_t are small and $\theta_0 = 0^\circ$ in Eq. (1), it leads to

$$\frac{d\theta_t}{dt} \approx -\frac{\gamma\left(\frac{\theta_t^2}{2r_0}\right)}{\zeta + \frac{6\eta\ln\left(\frac{x_{max}}{x_{min}}\right)}{\theta_t}} \tag{2}$$

where r_0 is the fiber radius. When the viscous dissipation is dominant (i.e., ζ is very small), we thus obtain

$$\theta_t \propto t^{-1/2} \tag{3}$$

and when frictional dissipation is dominant, Eq. (2) gives

$$\theta_t \propto t^{-1} \tag{4}$$

The validations of Eqs. (3) and (4) have been verified in experiments and molecular dynamics simulations [20–23].

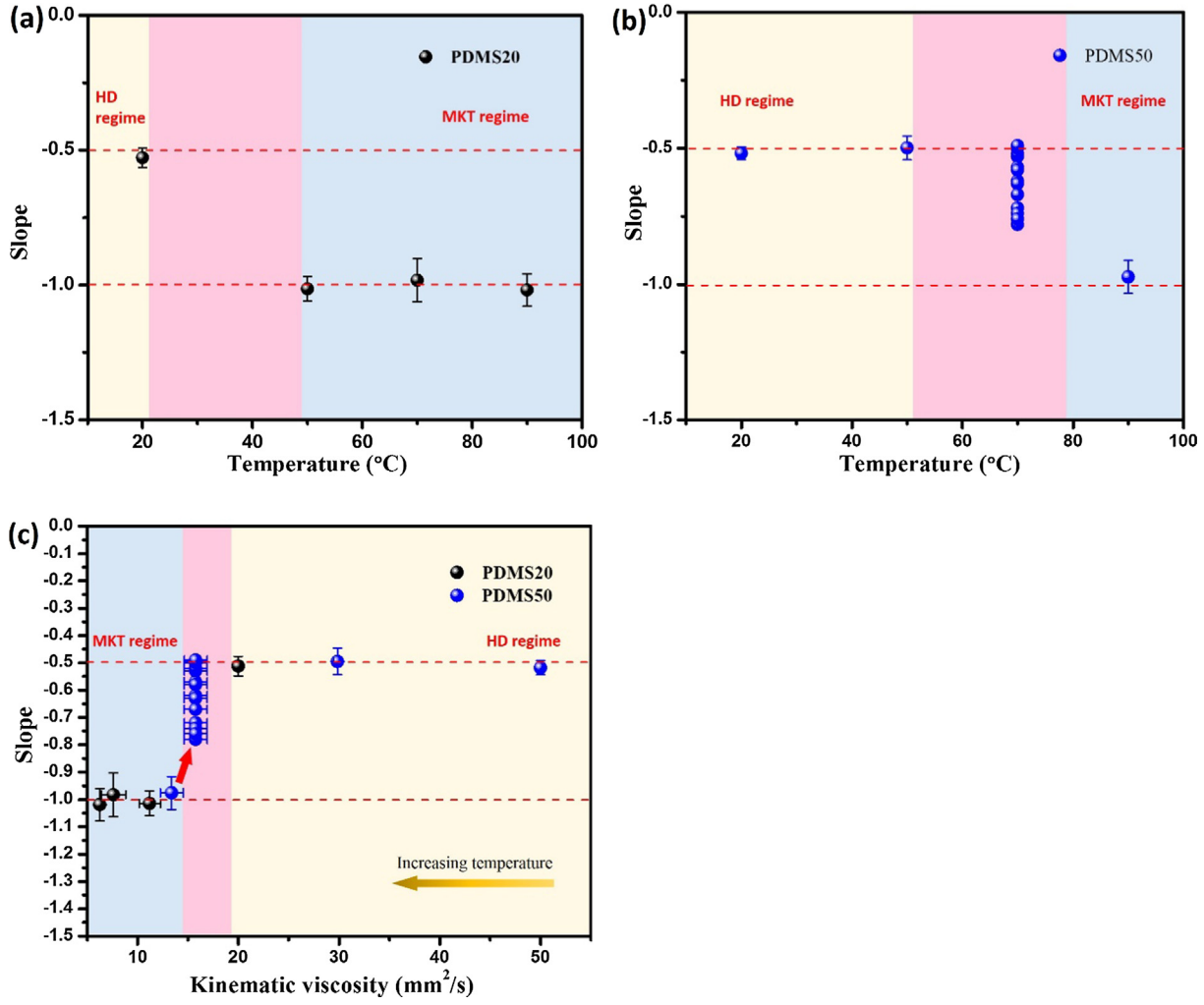

Fig. 7. Temperature dependence of slopes for PDMS20 (a) and PDMS50 (b). Viscosity dependence (c) of slope for PDMS20 and PDMS50.

3. Results and discussion

3.1. Dynamic contact angle relaxation

Fig. 4a and b show the contact angle relaxation of PDMS20 and PDMS50 at different temperatures, and the corresponding meniscus height dynamics are presented in Fig. 4c and d. It should be noted that the significant additional elastic stress does not exist during the breakup of the liquid/vapor interface due to the relatively low surface tensions of PDMS liquids (Fig. 1) [23]. It is expected that high temperature promotes the spreading process due to the sharp reduction of viscosity with temperature (Fig. 1). Interestingly, when temperature increases from 20 °C to 50 °C, the spreading process is improved dramatically and the contact angle relaxation is very close to the ones at 70 and 90 °C for PDMS20. PDMS50 in Fig. 4b and d shows similar spreading process with PDMS20 when temperature increases from 20 °C to 90 °C, except 70 °C. Actually, it is unexpected that the behaviors of contact angle relaxations (Fig. 4b) and height dynamics (Fig. 4d) show very large variations for PDMS50 at 70 °C even though the wetting experiments were repeated 20 times (see Fig. S3). For comparison and as an example, the wetting curves of PDMS50 at 50 °C is shown in Fig. S4, indicating a good repeatability. We select the upper and lower limiting dynamics enveloping all the other ones and plot them in Fig. 4b and d.

The same contact angle dynamics ($\theta_t \leq 45°$) are assessed on logarithmic scales in Fig. 5a and b. Except the case of PDMS50 at 70 °C (the slopes range from −0.75 to −0.5 in Fig. 5b), two different dynamic behaviors are presented when the system approaches equilibrium. Table 1 summarizes the two sets of slopes and deviations for PDMS20 and PDMS50. Apparently, the contact angle dynamics of PDMS20 at 20 °C, and PDMS50 at 20 °C and 50 °C follow the HD behavior ($\theta_t \sim t^{-1/2}$). On the other hand, the behaviors of PDMS20 at 50 °C, 70 °C and 90 °C, and PDMS50 at 90 °C can be described by the MKT model ($\theta_t \sim t^{-1}$). The evaluation of dynamic contact angles is performed below 45° here as the cosine function can then be approximated by the second Taylor expansion which is a requirement to derive the scaling laws ($\theta_t \sim t^{-1/2}$ and $\theta_t \sim t^{-1}$) in Eq. (2). Besides, independent tensiometric measurements of PDMS20 and PDMS50 (Fig. S5) confirm that the static contact angle θ_0 is equal to 0° at 20 °C, and hence the values of θ_0 are also considered to be 0° at higher temperatures [33].

It should be noted that dynamic contact angles at higher temperatures are evaluated with lower contact angles (Fig. 5a), because liquids with lower viscosities can be more easily affected by inertia and its effect should be eliminated from the analysis. The meniscus rise of liquid on a small fiber driven by inertia [21] can be described by

$$y_t \approx \alpha\left(\frac{\gamma r_0 t^2}{\rho}\right)^{1/4} \tag{5}$$

and it is equivalent to

$$\ln y_t = \frac{1}{2}\ln t + \ln\frac{\alpha\gamma^{1/4} r_0^{1/4}}{\rho^{1/4}} \tag{6}$$

where α is an adjustable parameter and ρ is the liquid density. The logarithms of the meniscus height for PDMS20 at different temperatures are presented in Fig. 6. It suggests that the early stages of the meniscus rise of PDMS20 obey Eq. (6) and they are thus dominated by inertia. Accordingly, the scaling laws do not model dynamic angle relaxations in Fig. 5a and b until the elimination of inertial effects.

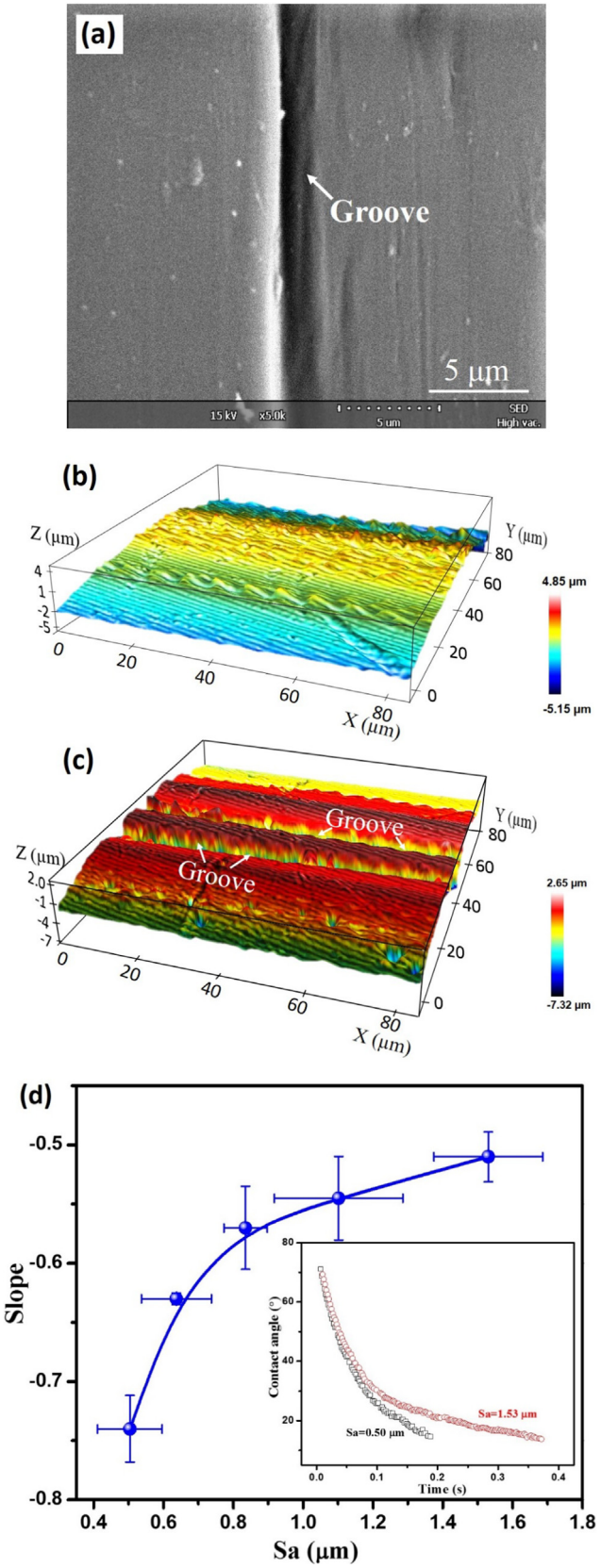

Fig. 8. (a) SEM image of PET fiber evidencing the presence of a groove on the surface. (b) and (c) Two typical 3D profiler images of fiber surfaces, the values of their roughness Sa are respectively 0.782 and 1.506 μm. (d) Slop versus Sa for PDMS50 at 70 °C. The inset in (d) shows two contact angle relaxations with various roughness values.

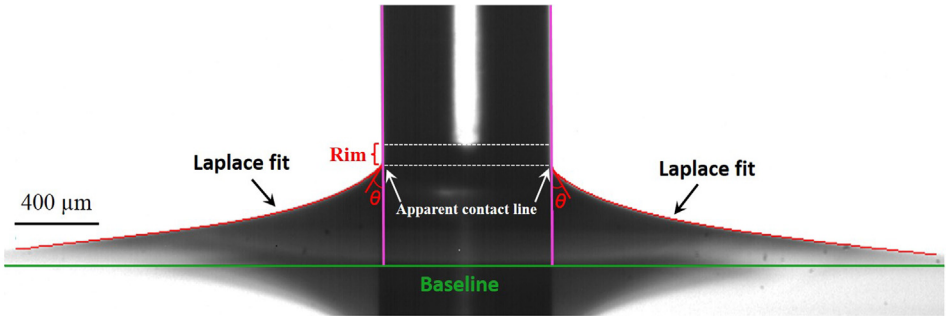

Fig. 9. A typical optical image of a meniscus of PDMS50 at 20 °C. A clear rim exists ahead of the apparent contact line.

3.2. The viscosity dependence of the wetting dynamic regimes

Fig. 7a and b depict the slopes of the scaling laws versus temperature for PDMS20 and PDMS50. It suggests that the slope changes from −0.5 to −1 with increasing temperature, implying a transition between the channels of dissipation. It should be noted that varying the temperature here is an efficient method to fine-tune the liquid viscosity. Essentially, the decreasing viscosity leads to the switch from viscous bending to frictional dissipation. The viscosity dependence of slopes is presented in Fig. 7c. It can be observed that the MKT/HD transition is very narrow in terms of viscosities. The threshold is considered to be around 15.8 mm^2/s (the viscosity of PDMS50 at 70 °C), as the slope dramatically jumps towards -0.5 despite strong variation. This transition is very sharp, as the viscosity difference between 70 °C and 90 °C is only 2.4 mm^2/s. It is much sharper with a viscosity difference around 0.1 mm^2/s if the lower deviation of viscosity at 70 °C and the upper deviation of 90 °C for PDMS50 are taken into consideration. This finding is interesting as it reveals the deep relationship between the frictional and viscous dissipations, which, to the best of our knowledge, has never been considered so far. The extreme sharpness of this transition here may explain why it has never been observed before.

The reason of the behavior of PDMS50 at 70 °C (Figs. 4b and 5b) and the relationship between viscosity and slopes (Fig. 7c) however remain open questions. The topographical heterogeneities of the fibers may explain our intriguing results in Figs. 4b and 5b [33–36]. The surface topography of PET fiber is checked by SEM image in Fig. 8a. It indicates a microscale groove exists on the fiber surface and evidences the topographical heterogeneity of surface. Fig. 8b and c show two typical 3D profiler images of fibers on which the presence of grooves can be quantitatively characterized by the roughness parameter Sa (arithmetic average of the 3D roughness). Some very tiny grooves still are visible in the top view image of Fig. 8b (see Fig. S6a in supplementary material). It should be noted that the value of Sa reflects the number of grooves as well as their width and depth, as supported in Fig. S6b–d (see Text S6). Slope values have a clear tendency to increase with roughness values as evidenced by Fig. 8d. We hypothesize that the capillary flow in the microscale grooves cannot contribute to the acquisition of apparent contact angles, but it will take on the partial dissipation of energy for the whole system. This causes a reduction of the apparent spreading velocity, as demonstrated by the inset of Fig. 8d that shows a slower contact angle relaxation with an increasing roughness. This is analogous to the situation that a tributary or subterranean flow reduces flow velocity of a main stream.

Concerning the link between slopes and viscosity, it may be understood in terms of the formation of rims ahead of the apparent contact line, as illustrated in Fig. 9. Apel-Paz and Marmur [37] suggested that there is a competition between the velocity of the apparent contact line (*Va*) and the velocity of the rim (*Vr*) on rough surfaces. The grooves on PET fiber can trigger the formation of groove capillary flows on the surface (Fig. 8a–c). Indeed, these microscale groove capillaries can be fed with liquid by the edge of the apparent contact line and spread simultaneously with the penetration of the liquid into the grooves, as supported experimentally by Oliver and Mason [38] and theoretically by Romero et al. [39]. If *Va* is faster than *Vr*, no rim is formed (see Fig. 3). At such high *Va*, the PDMS liquid does not perceive the surface roughness and spreads as if the surface were smooth. This statement is supported by the work of Cazabat et al. [40]. It gives rise to the viscosity-independent MKT regime (Fig. 7c). If *Va* is lower than *Vr*, rims exist due to the surface grooves (Fig. 9). It is noted that the rim exists during the whole wetting process (see Fig. S7). The role of the rim is very analogous to a precursor film in front of the contact line of a droplet where there is strong viscous dissipation [1]. Besides, the true contact line at the leading edge of the rim does not play a part in the creation of the apparent contact angle that is measured, and hence the conditions for the MKT are not realized [13]. Moreover, the liquid in grooves smooth out the surface roughness [41], and the liquid meniscus actually spreads on a partially pre-wetted solid surface. This reduces the influence of heterogeneous topographies on the apparent flow of liquid, resulting in the viscosity-independent HD regime (Fig. 7c). However, when *Va* and *Vr* are close, a sharp transition appears. In such condition, the wetting dynamics is sensitive to surface topographies and its heterogeneity induces irregular fluctuations of the relationship between *Va* and *Vr*, leading naturally to the combination of the MKT and HD scaling laws with slopes ranging between −0.75 and −0.5 in the present work.

4. Conclusions

The dynamics of the capillary rise of PDMS20 and PDMS50 on a PET fiber is studied at different temperatures and the results confirm that either the MKT or HD approach can model the spontaneous rise phenomenon. It also suggests that varying the temperature is a way to control the viscosity-tunable channels of dissipation. More importantly, the transition between the HD and MKT regimes lies in a very short viscosity interval. Within this sharp transition region, the fiber roughness plays an important role in the identification of the dominant channels of dissipation, whereas they are independent of fiber roughness beyond this transition region. The formation of rims ahead of the apparent contact line is observed and it can account for the link between the channels of dissipation.

The deep relationship between the two models was nearly not considered in the previous works even though the suitability or superiority of the two models was studied extensively [4,18,31,42,43]. In the present work, a sharp transition region linking the two models is uncovered experimentally and we propose a

qualitative explanation for the sharp MKT/HD transition by describing the relationship between *Va* and *Vr*. A theoretical basis conciliating the MKT and HD more tightly than the existing combined models [25–27] should provide a more quantitative description. However, modelling this transition goes beyond the scope of this work. We believe that the experimental characterization of this link is an important step to better understand the tight relationship between the frictional and viscous dissipations and it may serve as the basis for the formulation of a still missing unified wetting approach. More elaborated theoretical developments considering the surface topography and its effect on the different channels of dissipation are however still necessary. It will be the purpose of future works.

Acknowledgments

We gratefully acknowledge Dr. T.D. Blake for fruitful discussions and invaluable comments on this manuscript. Thanks are also given to Dr. E. Gosselin, Mr. M. Amin Ali, Mr. A. Vandaele and Mr. S. Waeyenbergh for their helps in experiments. This research has been partially funded by the Interuniversity Attraction Poles Programme (IAP 7/38 MicroMAST) initiated by the Belgian Science Policy Office.

Appendix A. Supplementary material

Supplementary data to this article can be found online at https://doi.org/10.1016/j.jcis.2018.10.082.

References

[1] P.G. de Gennes, Wetting: statics and dynamics, Rev. Mod. Phys. 57 (3) (1985) 827–863.
[2] D. Bonn, J. Eggers, J. Indekeu, J. Meunier, E. Rolley, Wetting and spreading, Rev. Mod. Phys. 81 (2) (2009) 739–805.
[3] J. De Coninck, T.D. Blake, Wetting and molecular dynamics simulations of simple liquids, Annu. Rev. Mater. Res. 38 (2008) 1–22.
[4] E. Saiz, A.P. Tomsia, Atomic dynamics and Marangoni films during liquid-metal spreading, Nat. Mater. 3 (12) (2004) 903–909.
[5] S. Lim, H. Zhang, P. Wu, A. Nikolov, D. Wasan, The dynamic spreading of nanofluids on solid surfaces–role of the nanofilm structural disjoining pressure, J. Colloid Interface Sci. 470 (2016) 22–30.
[6] D. Brutin, V. Starov, Recent advances in droplet wetting and evaporation, Chem. Soc. Rev. 47 (2) (2018) 558–585.
[7] C. Huh, L. Scriven, Hydrodynamic model of steady movement of a solid/liquid/fluid contact line, J. Colloid Interface Sci. 35 (1) (1971) 85–101.
[8] O. Voinov, Hydrodynamics of wetting, Fluid Dyn. 11 (5) (1976) 714–721.
[9] L. Tanner, The spreading of silicone oil drops on horizontal surfaces, J. Phys. D: Appl. Phys. 12 (9) (1979) 1473.
[10] R. Cox, The dynamics of the spreading of liquids on a solid surface. Part 1. Viscous flow, J. Fluid Mech. 168 (1986) 169–194.
[11] T.D. Blake, J.M. Haynes, Kinetics of liquid/liquid displacement, J. Colloid Interface Sci. 30 (3) (1969) 421–423.
[12] T.D. Blake, Dynamic contact angles and wetting kinetics, in: J.C. Berg (Ed.), Wettability, Marcel Dekker, New York, 1993, pp. 251–309.
[13] T.D. Blake, The physics of moving wetting lines, J. Colloid Interface Sci. 299 (1) (2006) 1–13.
[14] R. Sedev, The molecular-kinetic approach to wetting dynamics: achievements and limitations, Adv. Colloid Interface Sci. 222 (2015) 661–669.
[15] D. Ausserré, A. Picard, L. Léger, Existence and role of the precursor film in the spreading of polymer liquids, Phys. Rev. Lett. 57 (21) (1986) 2671.
[16] M.J. de Ruijter, M. Charlot, M. Voué, J. De Coninck, Experimental evidence of several time scales in drop spreading, Langmuir 16 (5) (2000) 2363–2368.
[17] J. De Coninck, M.J. de Ruijter, M. Voué, Dynamics of wetting, Curr. Opin. Colloid Interface Sci. 6 (1) (2001) 49–53.
[18] Y. Zhang, C.A. Fuentes, R. Koekoekx, C. Clasen, A.W. Van Vuure, J. De Coninck, D. Seveno, Spreading dynamics of molten polymer drops on glass substrates, Langmuir 33 (34) (2017) 8447–8454.
[19] D. Seveno, A. Vaillant, R. Rioboo, H. Adao, J. Conti, J. De Coninck, Dynamics of wetting revisited, Langmuir 25 (22) (2009) 13034–13044.
[20] D. Quéré, J.-M. Di Meglio, The meniscus on a fibre, Adv. Colloid Interface Sci. 48 (1994) 141–150.
[21] C. Clanet, D. Quéré, Onset of menisci, J. Fluid Mech. 460 (2002) 131–149.
[22] D. Seveno, J. De Coninck, Possibility of different time scales in the capillary rise around a fiber, Langmuir 20 (3) (2004) 737–742.
[23] M.J. Vega, D. Seveno, G. Lemaur, M.H. Adão, J. De Coninck, Dynamics of the rise around a fiber: experimental evidence of the existence of several time scales, Langmuir 21 (21) (2005) 9584–9590.
[24] G. Lu, X.-D. Wang, Y.-Y. Duan, A critical review of dynamic wetting by complex fluids: from Newtonian fluids to non-Newtonian fluids and nanofluids, Adv. Colloid Interface Sci. 236 (2016) 43–62.
[25] P. Petrov, I. Petrov, A combined molecular-hydrodynamic approach to wetting kinetics, Langmuir 8 (7) (1992) 1762–1767.
[26] F. Brochard-Wyart, P.G. de Gennes, Dynamics of partial wetting, Adv. Colloid Interface Sci. 39 (1992) 1–11.
[27] M.J. de Ruijter, J. De Coninck, G. Oshanin, Droplet spreading: partial wetting regime revisited, Langmuir 15 (6) (1999) 2209–2216.
[28] E. Saiz, A. Tomsia, N. Rauch, C. Scheu, M. Ruehle, M. Benhassine, D. Seveno, J. De Coninck, S. Lopez-Esteban, Nonreactive spreading at high temperature: molten metals and oxides on molybdenum, Phys. Rev. E 76 (4) (2007) 041602.
[29] Y. Zhang, A. Vandaele, D. Seveno, J. De Coninck, Wetting dynamics of polydimethylsiloxane mixtures on a poly (ethylene terephthalate) fiber, J. Colloid Interface Sci. 525 (2018) 243–250.
[30] J.E. Mark, Physical properties of polymers handbook, Second ed., Springer, New York, 2007.
[31] M.J. Vega, C. Gouttiere, D. Seveno, T.D. Blake, M. Voué, J. De Coninck, A. Clarke, Experimental investigation of the link between static and dynamic wetting by forced wetting of nylon filament, Langmuir 23 (21) (2007) 10628–10634.
[32] P.G. de Gennes, Deposition of langmuir-blodgett layers, Colloid Polym. Sci. 264 (5) (1986) 463–465.
[33] G. Kumar, K.N. Prabhu, Review of non-reactive and reactive wetting of liquids on surfaces, Adv. Colloid Interface Sci. 133 (2) (2007) 61–89.
[34] M. Ramiasa, J. Ralston, R. Fetzer, R. Sedev, The influence of topography on dynamic wetting, Adv. Colloid Interface Sci. 206 (2014) 275–293.
[35] A.M. Karim, J.P. Rothstein, H.P. Kavehpour, Experimental study of dynamic contact angles on rough hydrophobic surfaces, J. Colloid Interface Sci. 513 (2018) 658–665.
[36] G. McHale, N. Shirtcliffe, S. Aqil, C. Perry, M. Newton, Topography driven spreading, Phys. Rev. Lett. 93 (3) (2004) 036102.
[37] M. Apel-Paz, A. Marmur, Spreading of liquids on rough surfaces, Colloids Surf. A 146 (1–3) (1999) 273–279.
[38] J. Oliver, S. Mason, Microspreading studies on rough surfaces by scanning electron microscopy, J. Colloid Interface Sci. 60 (3) (1977) 480–487.
[39] L. Romero, F. Yost, Flow in an open channel capillary, J. Fluid Mech. 322 (1996) 109–129.
[40] A.M. Cazabat, M.A. Cohen Stuart, Dynamics of wetting: effects of surface roughness, J. Phys. Chem. 90 (22) (1986) 5845–5849.
[41] P.G. de Gennes, F. Brochard-Wyart, D. Quéré, Capillarity and wetting phenomena: drops, bubbles, pearls, waves, Springer-Verlag, New York, 2004.
[42] P. Wu, A.D. Nikolov, D.T. Wasan, Capillary rise: validity of the dynamic contact angle models, Langmuir 33 (32) (2017) 7862–7872.
[43] M.F. Pucci, B. Duchemin, M. Gomina, J. Bréard, Temperature effect on dynamic wetting of cellulosic substrates by molten polymers for composite processing, Compos. Part A 114 (2018) 307–315.